The Relation between the Electrical, Chemical, and Morphological Properties of Indium–Tin Oxide Layers and Double-Layer Light-Emitting Diode Performance

ARTICLE *in* THE JOURNAL OF PHYSICAL CHEMISTRY C · OCTOBER 2007

Impact Factor: 4.77 · DOI: 10.1021/jp0744376

7 AUTHORS, INCLUDING:

Paolo Vacca
SAES Getters Group
33 PUBLICATIONS **634** CITATIONS
SEE PROFILE

Mario Petrosino
Università degli Studi di Salerno
23 PUBLICATIONS **128** CITATIONS
SEE PROFILE

Rosa Chierchia
ENEA
30 PUBLICATIONS **425** CITATIONS
SEE PROFILE

Alfredo Rubino
Università degli Studi di Salerno
66 PUBLICATIONS **531** CITATIONS
SEE PROFILE

The Relation between the Electrical, Chemical, and Morphological Properties of Indium−Tin Oxide Layers and Double-Layer Light-Emitting Diode Performance

Paolo Vacca,*,† Mario Petrosino,‡ Alfredo Guerra,† Rosa Chierchia,† Carla Minarini,† Dario Della Sala,† and Alfredo Rubino‡

ENEA Research Center Portici, via Vecchio Macello, 80055 Portici (NA), Italy, and Department of Information and Electrical Engineering, University of Salerno, via Ponte Don Melillo, 84084 Fisciano (SA), Italy

Received: June 8, 2007

The relation between the electrical, chemical, and morphological properties of indium−tin oxide (ITO) thin films and organic light-emitting diode (OLED) performance is studied. We report on chemical (HCl, piranha solutions), thermal (vacuum annealing), physical (oxygen plasma, UV ozone), and combined treatments on ITO layers. The effects of these different treatments have been studied using the four-point probe resistivity measurement method, contact angle measurement, X-ray diffraction, surface profilometry, and UV−vis−IR transmittance. Double-layer OLEDs with treated ITO as the anode and poly(9,9-dihexyl-9H-fluorene-2,7-diyl) and 8-hydroxyquinoline aluminum salt as the hole transporter and emitting material, respectively, have been realized. The electrical and optical properties of OLEDs have been extensively investigated, and it is shown that UV ozone−HCl combined treatment yields the highest hole injection efficiency and luminance and the lowest drive voltage. For each OLED with treated ITO, the anode potential barrier height decrease is estimated using Fowler−Nordheim and Schottky−Richardson modeling of the electrical conduction.

Introduction

A large variety of transparent conducting oxides have been developed for flat panel display technologies, but the anode of organic light emitting diodes (OLEDs) is commonly a thin layer of a indium−tin oxide (ITO). ITO has been, by far, the preferred choice because of its commercial availability, its good transparency in the visible range, and its low resistivity. Therefore, the relationships between the electrical, chemical, and morphological properties of ITO modified by various surface treatments and device performances have been widely studied.[1−8] Some authors have shown that the lifetime of multilayer OLEDs with a hole transporter layer (HTL) is not solely determined by the properties of the interface between the active material and the HTL, but it is also strongly influenced by the interface between the HTL and the electrode.[9] Indeed, surface treatments can increase ITO work function, probably because of surface carbon removal, the creation of surface dipoles, and changes in the ratio of the surface constituents.

However, published results are contradictory. In fact, the optimal reported treatment is dipping in acid followed by UV ozone exposure, for Li et al.[10] Oxygen plasma followed by aqua regia yields higher efficiency according to Kim et al.[4] This paper is a contribution to increase the understanding of some open question. We compare the effects of some ITO surface treatments on OLED performance: chemical (HCl, piranha solutions), thermal (vacuum annealing), and physical treatments (oxygen plasma, UV ozone), and a combination of them. Commercial ITO layers have been treated with the selected methods and have been characterized by using several techniques: four-point probe resistivity measurement, contact angle, X-ray diffraction (XRD), surface profilometry, and UV−vis−IR transmittance. Subsequently, OLEDs with the common structure ITO/ poly(9,9-dihexyl-9H-fluorene-2,7-diyl) (PF6)/ 8-hydroxyquinoline aluminum salt (Alq_3)/Al have been realized on the treated ITO layers, and their performance has been investigated by electrical and optical measurements.

Experimental Section

ITO Surface Treatments. Commercial ITO layers deposited on glass plate by Delta Technologies were cut into 50 × 50 mm samples. Five sets of samples (8 pieces each) underwent the following treatments:

(a) HCl solution (12% (v/v) HCl/water) acid treatment. The substrates were dipped in the solution at room temperature, for 15 min.

(b) "Piranha" solution (H_2SO_4/H_2O_2 4:1 (v/v)) acid treatment. The substrates were dipped in the solution at room temperature for 15 min.

(c) Oxygen plasma treatment. Pure oxygen gas was introduced into a plasma etch chamber with a 30 sccm flux and at a pressure of 0.2 mbar, at room temperature. The applied forward and reflected powers were 60 W and less than 1 W, respectively.

(d) UV ozone treatment. The substrates were exposed to a 50 W UV light source (wavelength range 250−300 nm) 10 cm away under oxygen flow for 30 min.

(e) Thermal treatment. The substrates were annealed in vacuum at 200 °C for 1440 min.

(f) Combined treatment. We used UV ozone first and HCl solution later, as these two treatments have been reported by many authors as the promoters of highest efficiency and luminance and lowest drive voltage.[10−11]

After all the treatments, ITO substrates were rinsed in distilled water and finally dried with nitrogen, immediately before OLED

* Corresponding author. Address: CR ENEA Portici, Via Vecchio Macello, 80055 Portici (NA), Italy. E-mail: paolo.vacca@portici.enea.it. Tel.: +39 081 7723386. Fax: +39 081 7723344.

† ENEA Research Center Portici.

‡ University of Salerno.

10.1021/jp0744376 CCC: $37.00
Published on Web 11/01/2007 PAGE EST: 4.6

TABLE 1: Summary of the ITO Parameters with Different Surface Treatments

ITO treatment	time (min)	R_s (Ω/□)	rms roughness (nm)	spikes (nm)	surface energy (mJ/m^2)	polarity X_p
untreated		10.55	2.4	17.2	32.56	0.49
UV ozone	30	10.00	3.0	24.9	34.40	0.52
HCl (12%)	15	12.31	3.1	14.5	42.36	0.31
UV ozone−HCl (12%)	30 + 15	11.13	2.6	9.4	46.60	0.51
annealing 200 °C	1440	10.33	2.5	11.9	36.34	0.48
oxygen plasma	5	10.44	1.8	11.0	38.72	0.65
piranha	15	10.03	4.5	10.7	63.08	0.58

deposition. The lengths of each treatment were previously optimized. ITO substrate properties without any treatment were used as a reference.

An extensive characterization was performed on each treated sample using the following methods:

(a) Contact angle measurements were performed by using Dataphysics OCA 20 equipment at 21 °C and 50% relative humidity. We used water (polar) and diiodomethane (nonpolar) solvents to evaluate the polar and dispersion components of the surface energy. The standard error of contact angle measurements was ±2°.

(b) The evaluation of the sheet resistance was carried out with the four-point probe technique.

(c) The crystal structure was determined by XRD measurements in classical $\theta-2\theta$ configuration with an MPD-XPERT (Philips) diffractometer using a Cu Kα radiation source.

(d) The film thickness and roughness were evaluated by a KLA Tencor P-10 surface profiler.

(e) The UV−vis and near-infrared (NIR) optical transmittance was measured with a Perkin-Elmer Lambda 900 spectrophotometer in the wavelength range of 400−2000 nm.

OLED Fabrication. Treated and untreated ITO substrates were utilized to realize "double-layer" OLED devices. ITO patterning was carried out by conventional photolithography to define the OLED geometry.

PF6 is a blue emitting polymer and is soluble in common organic solvents. It was used as a hole-transporting material, and a 1.0% (w/w) chlorobenzene solution with a 30 mJ/m^2 surface tension was spun over the substrates at 1000 rpm for 30 s. The spin coating process was developed using a Brewer Science Model 100 spin coater. After the deposition, the 70 nm thick films were baked in vacuum for 3 h at 50 °C.

Tris(8-hydroxy)quinoline aluminum (Alq_3), used as electron-transporting and emitting material, was deposited by thermal evaporation. The deposition process was performed in high vacuum at a base pressure of 10^{-7} mbar. The layer thickness was 60 nm. Al cathode, 200 nm thick, was evaporated as the final layer. The active device area was 12.57 mm.[2]

The device structure has not yet been optimized for the highest efficiency.

Current−voltage ($I-V$) characteristics were measured with a Keithley 4200 semiconductor characterization system in constant voltage mode, with logarithmic increment steps and a delay time of 200 ms before each measurement point.

The spectral radiance was monitored using a calibrated spectroradiometer by Optronics OL770. The OLED was mounted in front of the integrating sphere window in such a way that only the light emitted in the forward direction was detected. The spectral radiance determination allowed the calculation of the chromaticity coordinates (CIE) of the Alq_3 emission: $x = 0.3204$, $y = 0.5526$, and $z = 0.1236$. All the characterization was performed in air.

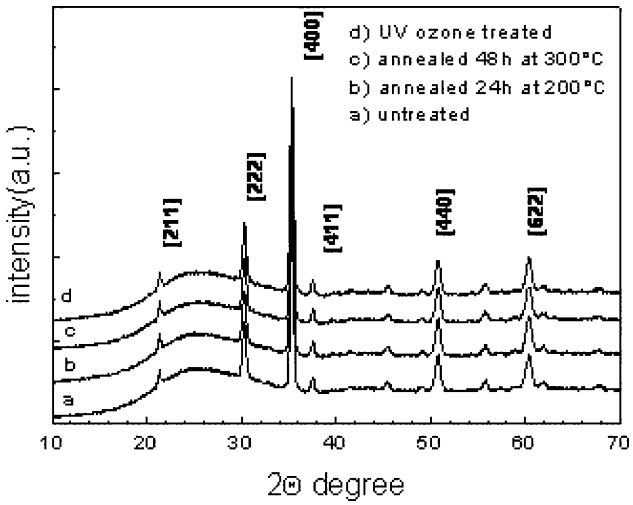

Figure 1. XRD patterns for different surface treatments of ITO.

Results and Discussion

ITO Surface Treatments. We have investigated the effect of different surface treatments on the ITO properties. In Table 1, sheet resistance, surface roughness, spike height, surface energy, and the polar component measurements for all the analyzed ITO layers are summarized.

Only with UV ozone (30 min) and piranha treatments has an appreciable decrease of sheet resistance been measured. Oxygen plasma is the only one whose effect is to planarize the ITO surface decreasing the root-mean-square (rms) surface roughness, in accordance with Kim et al.,[2−4] while surface roughness increases after UV ozone and HCl (12%) treatments and more noticeably with piranha. Concerning the height of the ITO spikes, all treatments except UV ozone give rise to a decrease, more significantly for combined UV ozone−HCl and for piranha treatments. This indicates that acid treatments produce some selective etching of the surface, and they are likely able to alter the heterogeneous surface composition.[2] For the combined UV ozone and HCl treatment, this phenomena is amplified from the oxidizer effect of the UV ozone.

We suppose that the spike height is more important than the rms value for device performances.[12] The reduction of spike height is very important to avoid the shorting effect, which promotes the formation of dark spots. Indeed, as some authors have pointed out, the ITO surface spikes have an important role in the device degradation.[13−14] Instead, some roughness could promote the active layer adhesion.

The XRD patterns of treated ITO layers are shown in Figure 1. We have analyzed only the samples that could have changed their crystalline structure (i.e., annealed and UV ozone). All samples show a cubic structure with diffraction peaks corresponding to (2 1 1), (2 2 2), (4 0 0), (4 1 1), and (6 2 2) in agreement with other authors,[13] without any significant change. This is probably due to the highly crystalline structure of the starting ITO layer. These results are in agreement with the transmittance spectra in the visible and NIR regions (Figure 2). For wavelengths below 1000 nm, the sample transmittance is unchanged, and, since the transmittance of ITO layers in this range is related to the grain-boundary scattering,[14] the grain size of the ITO film is not altered.

We have also investigated the wettability of the ITO layers by means of contact angle measurements. A substrate with a surface tension higher than the surface tension of the spin-coated solution (30 mJ/m^2 for PF3) induces a better wettability and a smaller contact angle and, at last, a better adhesion. In detail,

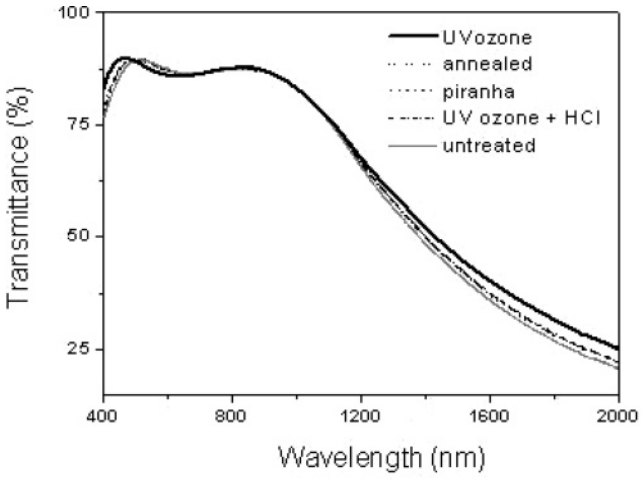

Figure 2. Transmittance vs wavelength on ITO at various surface treatments.

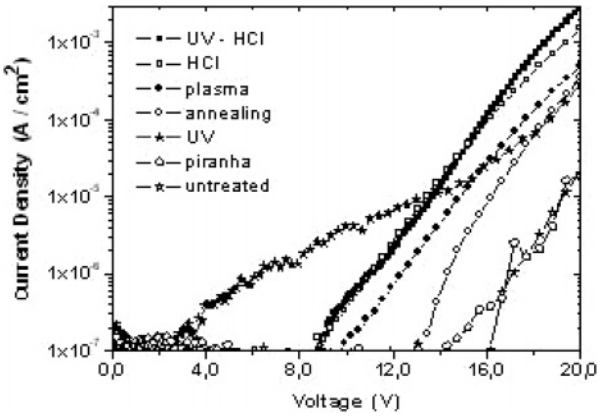

Figure 3. Current−voltage characteristics of OLEDs.

the contact angle (θ) between a flat solid surface and a liquid droplet is given by the Young equation as follows: $\gamma_S = \gamma_{SL} + \gamma_L \cdot \cos\theta$ where γ_S denotes the surface energy of the solid surface, γ_L is the surface tension of the liquid droplet, and γ_{SL} is the interfacial surface tension. Four types of van der Waals interactions contribute to the surface energy. In particular, the polar component results from three different intermolecular forces due to hydrogen bonding, permanent and induced dipoles, while the dispersion (nonpolar) component of the surface energy is due to instantaneous dipole moments also called London forces.[15] The ratio of the polar component to the total surface energy is reported as the *polarity* (X_p). In our study, all treatments produce an increase of the surface energy, while polarity reduces with HCl treatment, it stays constant with annealing, and it increases with all other treatments giving a result higher than that for oxygen plasma. We can suppose that the increased surface energy results mainly from the remotion of residual organics on ITO substrates because they are known to have low surface tensions.[16−17] At the same time, an increased polarity is due to an increased concentration of water that is physi- and/or chemisorbed on the surface. We believe that both these parameters (surface energy and polarity) are very important to achieve a better adhesion at the ITO/polymer interface. Differences between our study and the results obtained from other authors about surface roughness can be attributed to differences in the treatments procedure, different treatment times, and different starting parameters of the ITO.[4]

Organic Light-Emitting Diodes. In Figures 3and 4, the current−voltage and luminance−voltage characteristics of the realized devices are respectively reported. Since the devices are

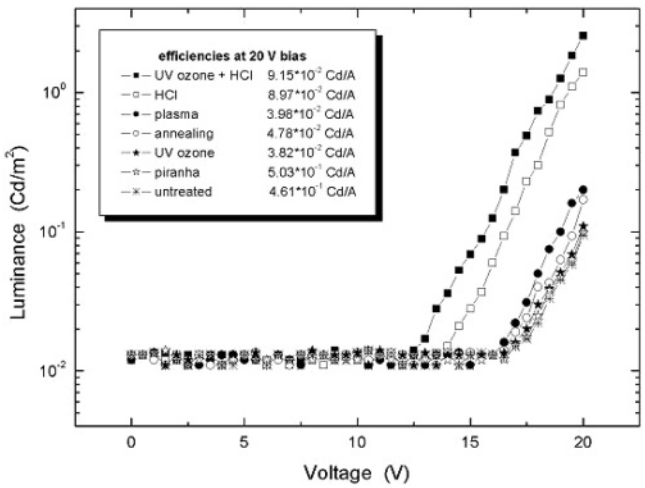

Figure 4. Luminance−voltage characteristics. In the inset, the current efficiency values for 20 V of applied voltage are reported.

TABLE 2: Interface Electrical Models[a]

eq 1[b]	$J = A^* T^2 \exp\left[- q\varphi_e / kT \right] \exp\left[qV / nkT \right]$
eq 2[c]	$J = A^* T^2 \exp\left[- q / kT \left(\varphi_e - \sqrt{qF / 4\pi\epsilon} \right) \right]$
eq 3[d]	$J = q^3 / 16\pi^2\hbar(q\varphi_e) F^2 \exp\left[- 4\sqrt{2m^*}(q\varphi_e)^{3/2} / 3q\hbar F \right]$

[a] J is the current density, V is the applied voltage, A^* is the Richardson constant, q is the electron charge, k is the Boltzmann constant, $\hbar$ is the Dirac constant, ϵ is the effective dielectric constant, F is the applied electrical field, n is the ideality factor, m^* is the free electron mass, T is the absolute temperature, and φ_e is the potential barrier. [b] Thermionic model. [c] Schottky−Richardson model. [d] Fowler−Nordheim model

equal in all features except ITO surface treatment, changes in the electro-optical behavior can be attributed just to ITO surface change properties.[18] Notice that all the treatments improve OLED conductivity and luminance. The optical threshold voltage is 17 V for the untreated sample, and it decreases according to the increase in the surface energy of treated ITO and the related device conductivity. The optical threshold reaches the minimum value of 12.6 V for the UV−HCl combined treatment (Figure 4).

The experimental $I-V$ curves reported in Figure 3 were fitted for bias higher than 8 V according with the equations in Table 2 (symbol specification is in the Table 2 footnote). These equations refer to the thermionic, Schottky−Richardson, and Fowler−Nordheim models, respectively. The low voltage range can be described with an ohmic regime followed by a space charge limited current behavior.

The thermionic model is not suitable to describe current−voltage characteristics because the range of values of the ideality factor (n in eq 1, Table 2) obtained fitting the experimental data is in the range of 96−128, and so it has no physical sense. On the contrary, both the Schottky−Richardson and Fowler−Nordheim models well describe the high-voltage branch of $I-V$ characteristics.

Plotting $\ln(I)$ versus $V^{1/2}$, a straight line is obtained in the high-field branch, as shown in Figure 5; by fitting these straight lines with eq 2 in Table 2, we obtain the slope ($q/kT\sqrt{q/4\pi\epsilon}$) and the intercept ($\ln(A^*T^2) - q/kT\varphi_e$) for each treatment. It is interesting to note that the slopes are equal within 10% (this is correct because they depend on bulk polymer properties through ϵ), while the intercepts contain the ITO/polymer interface barrier height φ_e and therefore they depend on the treatment. If we denote as b_0 the intercept for the untreated substrate, the potential

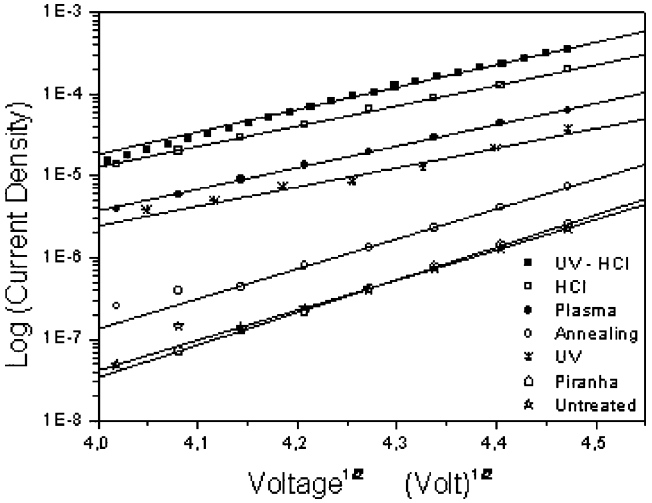

Figure 5. Schottky−Richardson fit for various ITO treatments.

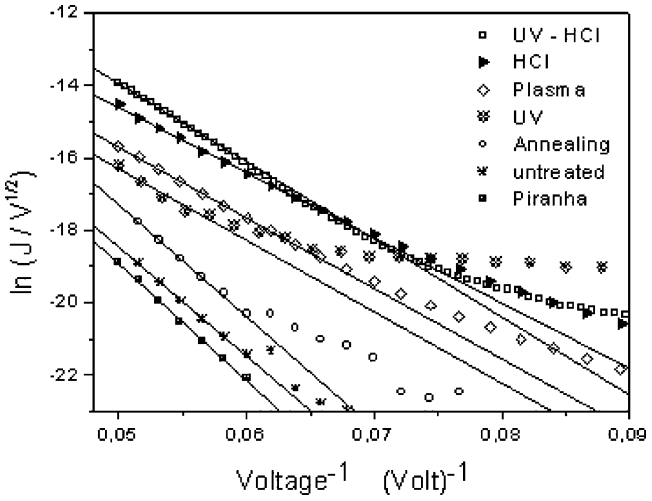

Figure 6. Fowler−Nordheim plot for various ITO treatments.

barrier change can be obtained according to the following equation:

$$\Delta\varphi_{\mathrm{eSR}} = \frac{kT}{q}(b_i - b_0) \tag{1}$$

where $\Delta\varphi_e$ is the potential barrier variation, SR indicates Schottky−Richardson model, and b_i is the line's intercept obtained after each treatment.

A straight line is also obtained plotting $\ln(I/V^2)$ versus V^{-1} in the high-field branch, as shown in Figure 6. These curves have been fitted with eq 3 in Table 2. In this case, the potential barrier variation can be obtained from the difference between the straight-line slopes: $-4\sqrt{2m^*}(q\varphi_e)^{3/2}/3q\hbar$. It has to be pointed out that the same information could also be obtained from the intercepts, but the slope results are free of any area variation dependence. Therefore,

$$\Delta\varphi_{\mathrm{eFN}} = \left(\frac{a_i}{Bd}\right)^{2/3} - \left(\frac{a_0}{Bd}\right)^{2/3} \tag{2}$$

$$B = 8\pi(2m^*)^{1/2}/3hq \tag{3}$$

In the above equations, d is the active device thickness (PF6 + Alq_3), a_0 is the line's slope for untreated ITO, and a_i is the line's slope for treated ITO substrates. The true value of the Bd product does not matter in the following discussion because it

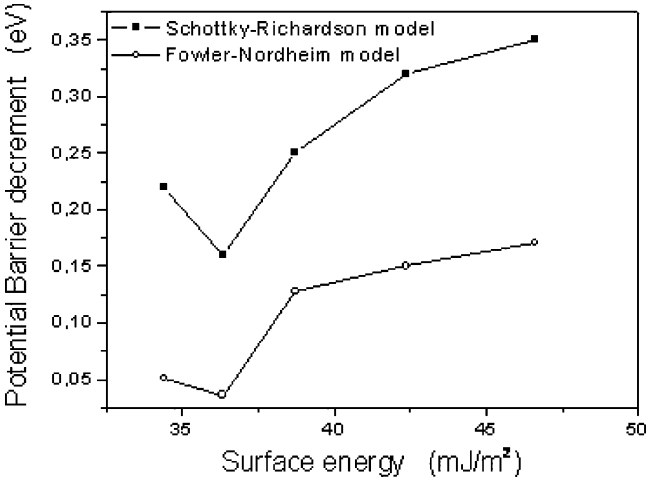

Figure 7. Potential barrier decrease vs surface energy obtained by Schottky−Richardson and Fowler−Nordheim model fitting; zero decrease is referred to the untreated sample.

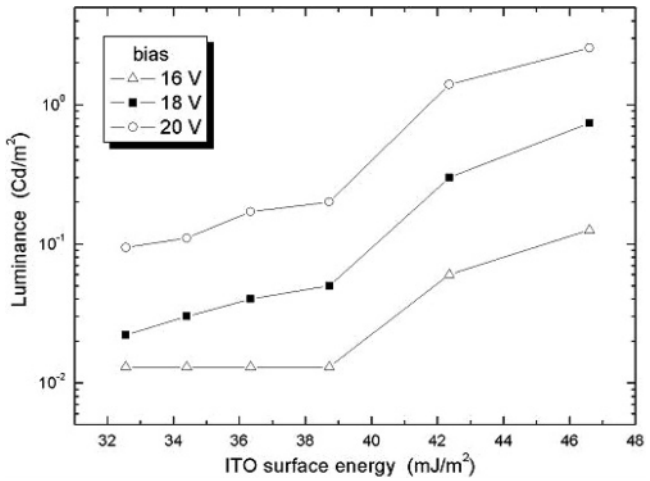

Figure 8. Brightness as a function of surface energy.

is only a scale factor. In Figure 7, the potential barrier decreases obtained according to the Schottky−Richardson and Fowler−Nordheim models are plotted versus surface energy; zero decrease is referred to the untreated sample. Both models have the same qualitative trend for the barrier height decrease.

Except for the UV treatment value (surface energy = 34.4 mJ/m^2), from Figure 7 we can deduce that by increasing the surface energy of substrates, the ITO/PF6 "effective" barrier height decreases. This probably correlates to a better adhesion of the polymeric HTL and subsequent reduction of the interfacial tension between the hole transporter material and the substrate.[19] The result is a better electrical contact between the two materials with a direct improvement of charge-carrier injection through the interface and therefore of the LED performances through an improvement of luminance and a decrease of optical voltage threshold. Concerning the UV treatment, barrier decrement is altered by a higher current value due to the high surface roughness and spike (see Table 1). The effects of these two surface characteristics are visible also at low bias (Figure 3) where this treatment gives the highest current.

It has to be stressed that no correlation has been found between ITO−PF6 barrier decrement and changes in the disperse and polar components of the ITO surface energy, substrates roughness, and spikes.

Figure 8 shows the device luminance versus the surface energy at three different biases: as the ITO surface energy increases, the device luminance increases.

In this discussion, the datum for piranha treatment has been omitted because, in this case, there is too high of a difference between the surface energy of the ITO and the surface tension of the employed chlorobenzene solution that destabilizes a uniform spreading of the polymer solutions.[20] In the future, the effect of piranha treatment will be examined with solutions with higher surface tension solutions (water PEDOT dispersions or alcohol solutions).

Finally, in the inset of Figure 4, the efficiency measured at 20 V is also reported. These values do not follow the same trend as the luminance; on the contrary, it seems that the devices with the piranha treatment and the untreated sample have the highest efficiencies, but it must be pointed out that these values are not optimized. This work is focused on a comparison between different ITO treatments and their effects on hole-injection efficiency; therefore any discussion on OLED efficiency should consider that the treatments give rise to an increase in the hole injection and, accordingly, in the hole current through the device. At the same time, the electron current is unaffected, so that the total device current increases, but the efficiency does not necessarily have the same behavior: the hole−electron recombination is limited by the not yet optimized electron current. It is known that the aluminum top contact gives rise poor electron injection, and, in order to improve it, the insertion of a thin intermediate Li layer or Mg/Al contact is necessary, so the efficiency will increase.

Therefore, the device luminance increases less than the device current, but the beneficial effect of the treatments is nevertheless clear. These remarks do not, however, invalidate the above discussion on the ITO surface properties effects.

Conclusions

In this work we have investigated the effects of acid, thermal, and physical treatments on ITO layers. The most important parameters (between the measured ones) seem to be the surface roughness and surface energy. In fact, both, giving rise to better adhesion, increase device conductivity and luminance, as shown in the electro-optical characteristics of diodes realized using PF6 as the hole-transporter material and Alq_3 as the active layer. The most significant improvements have been observed for the UV ozone + HCl-treated samples. They can be explained in terms of enhancement of the hole injection from the anode, favored by a decrease in the effective ITO/polymer barrier height, as inferred fitting the high-field current−voltage characteristics by means of the Fowler−Nordheim and Schottky−Richardson electrical transport models. Both models give the same qualitative estimation for barrier decrease, showing a higher decrease for the UV ozone + HCl treatment.

Acknowledgment. Support by the TRIPODE project financed by the Ministero dell'Università e della Ricerca (MIUR) is gratefully acknowledged.

References and Notes

(1) Utsumi, M.; Matsukaze, N.; Kumagai, A.; Shiraishi, Y.; Kawamura, Y.; Furusho, N. *Thin Solid Films* **2000**, *363*, 13.
(2) Kim, J. S.; Granstrom, M.; Friend, R. H.; Johansson, N.; Salaneck, W. R.; Daik, R.; Cacialli, F. J. *Appl. Phys.* **1998**, *84*, 6859.
(3) Kim, J. S.; Cacialli, F.; Cola, A.; Gigli, G.; Cingolani, R. *Synth. Met.* **2000**, *363*, 111.
(4) Kim, J. S.; Cacialli, F.; Cola, A.; Gigli, G.; Cingolani, R. *Appl. Phys. Lett.* **1999**, *75*, 19.
(5) Kim, J. S.; Friend, R. H.; Cacialli, F. J. *Appl. Phys.* **1999**, *86*, 2774.
(6) Nuesch, F.; Forsythe, E. W.; Le, Q. T.; Gao, Y.; Rothberg, J. J. *Appl. Phys.* **2000**, *87*, 7973.
(7) Lee, C. T.; Yu, Q. X.; Tang, B. T.; Lee, H. Y. *Thin Solid Films* **2001**, *386*, 105.
(8) You, Z. Z.; Dong, J. Y. *Appl. Surf. Sci.* **2005**, *249*, 271.
(9) Kim, J. S.; Friend, R. H.; Cacialli, F. *Appl. Phys. Lett.* **1999**, *74*, 3084.
(10) Li, C. N.; Djurisic, A. B.; Kwong, C. Y.; Lai, P. T.; Chan, W. K.; Liu, S. Y. *Appl. Phys. A* **2005**, *80*, 301.
(11) Li, C. N.; Kwong, C. Y.; Djurisic, A. B.; Lai, P. T.; Chui, P. C.; Chan, W. K.; Liu, S. Y. *Thin Solid Films* **2005**, *477*, 57.
(12) Tak, Y. H.; Kim, K. B.; Park, H. G.; Lee, K. H.; Lee, J. R. *Thin Solid Films* **2002**, *411*, 12.
(13) Hu, Y.; Diao, X.; Wang, C.; Hao, W.; Wang, T. *Vacuum* **2004**, *75*, 183.
(14) Wu, W. F.; Chiou, B. S. *Appl. Surf. Sci.* **1993**, *68*, 497.
(15) Ruckenstein, E.; Gourisankar, S. V. J. *Colloid Interface Sci.* **1986**, *109*, 557.
(16) Dan, L.; Ying, W.; Jianhua, G.; Guang, L.; Yue, W.; Jiacong, S.*Mater. Sci. Eng. B* **2003**, *97*, 141.
(17) So, S. K.; Choi, W. K.; Cheng, C. H.; Leung, L. M.; Kwong, C. F. *Appl. Phys. A* **1999**, *68*, 447.
(18) Zhong, Z. Y.; Jiang, Y. D. *Appl. Surf. Sci.* **2005**, *249*, 271.
(19) Nguyen, T. P.; Le Rendu, P.; Dinh, N. N.; Fourmigué, M.; Mézière, C. *Synth. Met.* **2003**, *138*, 229.
(20) Ma, K. X.; Ho, C. H.; Zhu, F.; Chung, T. S. *Thin Solid Films* **2000**, *371*, 140.